

Research note

Comparison of the Performance of Different Reverse Osmosis Membrane Modules by CFD Modeling

M. Bahoosh¹, E. Kashi^{1*}, S. Shokrollahzadeh¹, Kh. Rostami²

¹ Department of Chemical Technologies, Iranian Research Organization for Science and Technology (IROST), P. O. Box: 33535111, Tehran, Iran

² Department of Biotechnology, Iranian Research Organization for Science and Technology (IROST), P. O. Box: 33535111, Tehran, Iran

ARTICLE INFO

Article history:

Received: 2018-10-13

Accepted: 2018-11-07

Keywords:

CFD Modeling,
Desalination,
Pressure-Driven
Membrane,
Reverse Osmosis,
Solution-Diffusion

ABSTRACT

Reverse osmosis is a commonly used process in water desalination. Due to the scarcity of freshwater resources and wastewater problems, many theories and experimental studies have been implemented to optimize this process. In the present study, the performance of reverse osmosis membrane module of salt-water separation was simulated based on computational fluid dynamics technique and solution-diffusion theory. Eight geometries of membrane modules, four flat sheets, and four tubular membranes were investigated. It was found that if the membrane surface area and inlet flow rate were kept constant for the eight modules, the pressure drop and permeated flow rate would be approximately similar for some geometries (e.g., the performance of primary flat sheet channel is the same as 3 tubular membranes with $R=1/3 R_{ref}$). The results also showed that because of the phenomenon of concentration polarization, if it is possible to use more membranes with a smaller length, it can reduce the pressure drop and increase the permeation flux of water. Furthermore, the results showed that between the tubular and the plate membranes in similar conditions, the tubular one is more suitable for the water permeation due to its ease of construction and its ability to withstand ECP.

1. Introduction

Freshwater scarcity has become a major threat in the 21st century for many reasons, such as population growth, declining rainfall, and climate change. Desalination of sea and saline water and certain wastewater at present has strong potential to overcome the scarcity of water in many parts of the universe. According to a conventional classification,

the water desalination process consists of two groups: membrane methods (such as nanofiltration (NF) and reverse osmosis (RO)) and thermal methods (such as vapor condensation and multi-stage flash) [1–3]. Osmosis is defined as the movement of water through a selective semipermeable membrane due to the osmotic pressure difference on both sides of the membrane [4]. During the RO

*Corresponding author: Kashi@irost.ir

process, the external pressure difference overcomes the osmotic pressure difference ($\Delta P > \Delta \pi$) [5]; consequently, the water flows through the semipermeable membrane from the feed side to the permeate side.

Among the osmotic methods, major theoretical or empirical studies have been carried out in RO [6]. There are many factors that affect the performance of the RO process. Modeling is one of the ways to understand how these factors can affect the system's performance. In general, for the modeling and simulation of the RO process, three different boundary conditions are employed to define the membrane performance. In the first case, which includes older assumptions, the membrane is deemed to be impermeable, meaning that it does not allow particles to pass through the membrane; however, the concentration of dissolved salt in water is considered constant on the membrane surface. Although this method is very simple, it does not fully predict what really happens in the membrane module [7-8]. In the second case, the membrane is considered as a permeable surface, yet with constant permeability. Although, in this approach, consideration of salt rejection leads to a closer similarity between the simulation data and experimental results, still, it does not possess enough precision to predict the membrane performance during the RO process [9-10]. In the third and the most recent method, the theory of Solution-Diffusion [11-12] is employed that considers an inconstant permeation rate for the membrane definition. In this method, unlike other methods, solute concentration on the membrane surface, osmotic pressure, density, and molecular diffusion coefficient in the solution bulk are considered as variable parameters. These assumptions significantly affect the flow rate

of water or the rejection of undesirable material through the membrane. Furthermore, it has been attempted to take into account the concentration polarization effects as resistance against the flow of permeating water using more advanced equations [6-13].

After selecting an appropriate boundary condition, the membrane operation procedure can be used for study by using computational fluid dynamics as a modeling tool. CFD, as a branch of fluid mechanics, can solve governing equations of a mechanical system by numerical methods [14]. This method can examine different membrane modules in various conditions by considering parameters such as gravity, concentration, type of flow regime, and membrane rejection. In addition, the relationship of these parameters with the hydrodynamic conditions, solution characteristics, membrane structure, and module geometry have been studied [15-17].

In this study, due to the rare investigations with regard to the comparative study among RO membrane modules, the reverse osmosis process is simulated using the theory of solution-diffusion and CFD technique. Eight distinctive membrane geometries (four flat sheet and four cylindrical membranes) have been considered in this study. The membrane performance (permeate flux and pressure drop) of each geometry has been compared.

2. Numerical methods and model verification

2.1. Governing equations and boundary conditions

The RO membrane is simulated in an isothermal and steady-state condition without implementing the gravity effects. The governing equations for the fluid flow in both 2D Cartesian coordinate's channels are the equations for conservation of mass,

momentum, and solute mass fraction (Eq. 1-4).

$$\frac{\partial \rho u}{\partial x} + \frac{\partial \rho v}{\partial y} = 0 \quad (1)$$

$$\begin{aligned} \frac{\partial \rho u^2}{\partial x} + \frac{\partial \rho uv}{\partial y} = & -\frac{\partial P}{\partial x} + 2 \frac{\partial}{\partial x} \left(\mu \frac{\partial u}{\partial x} \right) + \\ \frac{\partial}{\partial y} \left[\mu \left(\frac{\partial u}{\partial y} + \frac{\partial v}{\partial x} \right) \right] - & \frac{2}{3} \frac{\partial}{\partial x} \left[\mu \left(\frac{\partial u}{\partial x} + \frac{\partial v}{\partial y} \right) \right] - \\ \rho g_x \end{aligned} \quad (2)$$

$$\begin{aligned} \frac{\partial \rho uv}{\partial x} + \frac{\partial \rho v^2}{\partial y} = & -\frac{\partial P}{\partial y} + 2 \frac{\partial}{\partial y} \left(\mu \frac{\partial v}{\partial y} \right) + \\ \frac{\partial}{\partial x} \left[\mu \left(\frac{\partial u}{\partial y} + \frac{\partial v}{\partial x} \right) \right] - & \frac{2}{3} \frac{\partial}{\partial y} \left[\mu \left(\frac{\partial u}{\partial x} + \frac{\partial v}{\partial y} \right) \right] - \\ \rho g_y \end{aligned} \quad (3)$$

$$\begin{aligned} \frac{\partial \rho u m_A}{\partial x} + \frac{\partial \rho v m_A}{\partial y} = & \frac{\partial}{\partial x} \left[\rho D_{AB} \left(\frac{\partial m_A}{\partial x} \right) \right] + \\ \frac{\partial}{\partial y} \left[\rho D_{AB} \left(\frac{\partial m_A}{\partial y} \right) \right] \end{aligned} \quad (4)$$

Because gravity is not considered in this study, the amount of g_x and g_y is zero.

The water flow rate through the membrane is determined by the Darcy law, and its passage through the membrane is based on the Solution-Diffusion theory. According to the present theory, the water permeation (v_w) is calculated based on the pressure difference applied between the feed and the permeate channels (Eq. 5) [18].

$$v_w = k(\Delta P - \Delta \pi) \quad (5)$$

In this equation, ΔP represents the applied external pressure on the RO membrane (here, $\Delta P = 5 \times 10^5$ Pa), $\Delta \pi$ is the osmotic pressure difference, and k is a constant number calculated according to the pure solvent permeation rate (here, $k = 2 \times 10^{-10}$ m s⁻¹ Pa⁻¹) [19]. On the surface of the membrane, the tangential velocity (velocity in X direction) is considered zero (a nonslip condition applied), and the permeate velocity in the transverse direction (Y) is equal to $v = v_w$. The balance

between the diffusive and convective fluxes of solute mass fraction on the membrane surface is presented as Eq. (6):

$$\rho D_{AB} \frac{\partial m_A}{\partial y} + \rho_w m_{Aw} v_w R = 0 \quad (6)$$

Also, for the first part of this study, the membrane rejection (R) is considered to be 95 %.

At the inlet ($x = -L_{in}$), there is no velocity component in the transverse direction, and the component of velocity in the longitudinal direction is defined as a parabolic and fully developed flow in Eq. (7):

$$\begin{cases} u = 6\bar{u} \frac{y}{h} \left(1 - \frac{y}{h} \right) \\ v = 0 \\ m_A = m_{A0} \end{cases} \quad (7)$$

where \bar{u} is the average velocity (here, $\bar{u} = 0.002$ m/s). At the outlet of the feed channel ($x = L_{out}$), the gauge pressure is equal to zero (Eq. 8):

$$P = 0 \text{ bar} \quad (8)$$

In non-membrane walls, the non-slip conditions and lack of solute flux have been applied (Eq. 9).

$$\begin{cases} u = 0 \\ v = 0 \\ \frac{\partial m_A}{\partial y} = 0 \end{cases} \quad (9)$$

The relationship between some variable parameters that affect the RO process along the membrane module is given by Eq. (10-13) for the osmotic pressure (Pa), viscosity (Pa s), molecular diffusion of salt in water (m² s⁻¹), and solution density (kg m⁻³), respectively. It should be noted that these equations are valid for sodium chloride solution in water up to a mass fraction of 0.09 [20].

$$\pi = 805.1 \times 10^5 m_A \quad (10)$$

$$\mu = 0.89 \times 10^{-3} (1 + 1.63 m_A) \quad (11)$$

$$D_{AB} = \max(1.61 \times 10^{-9}(1 + 14m_A), 1.45 \times 10^{-9}) \quad (12)$$

$$\rho = 997.1 + 694 m_A \quad (13)$$

2.2. Case description

To test the validity of the RO membrane model, a chamber (Fig. 1) with the same feed rectangular channel used by Fletcher [21] and Wardeh [19] has been studied. Its characteristics are shown in Table 1. In this process, by going through the membrane, a part of the feed solution enters the permeate region, which is located in the lower part of

the chamber, and then drives out of the permeate outlet. The residual solution at the outlet of the feed channel is concentrated by sodium chloride because the RO membrane acts as a semipermeable wall and does not allow sodium chloride to exit across the membrane [19]. In the feed solution, the mass fraction of NaCl in pure water has been considered to be 0.002.

The reason for considering L_{in} and L_{out} at the inlet and outlet of the membrane chamber is to make sure that flow development and the boundary conditions are correctly implemented, respectively.

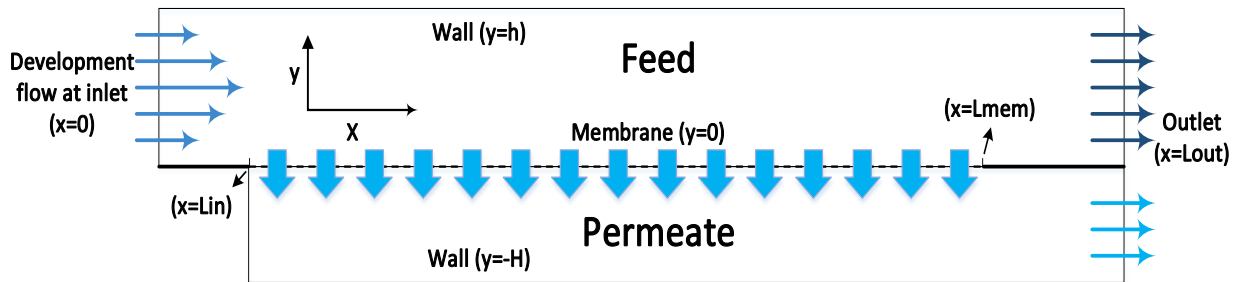


Figure 1. The geometry of the simulated membrane module [21].

Table 1

Characteristics of membrane modules (membrane length (from L_{in} to L_{mem}) is 250 mm).

| Length (x) | |
|----------------------|---------------|
| Parameter | Location (mm) |
| L_{in} | 20 |
| L_{mem} | 270 |
| L_{out} | 280 |
| Height (y) | |
| Feed channel (h) | 2 |
| Permeate channel (H) | -1.2 |

2.3. Geometry and mesh

Defining membrane geometry is one of the most important steps in the simulation. In this step, contrary to the previous simulations [19-21], the permeate section is removed, and the membrane geometry is shown in Fig. 2. There

are two critical assumptions behind this kind of geometry definition: first, the constant pressure in the permeate channel; second, the dependency of salt concentration at the membrane wall on the local flux of the solution (it means that the salt concentration

is not affected by the convective flow). The first assumption is only acceptable in modules with a smaller size than real RO modules, and the second one is suitable for a low

permeating flux through the RO process (about 10 % of the flux in the feed channel) [22].

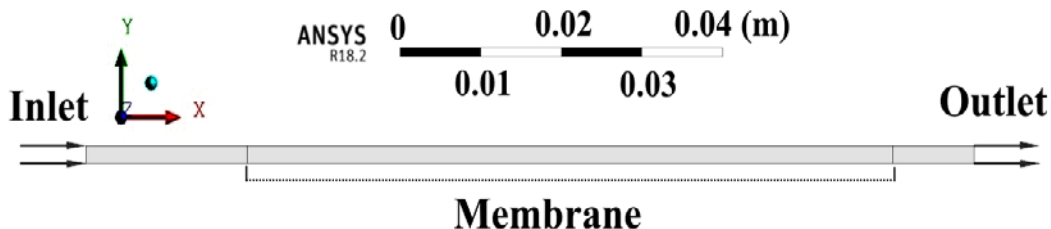


Figure 2. The Geometry of the membrane chamber.

The precision of the mesh and the governing conditions of the problem have a great effect on the simulation results. Increasing the mesh accuracy, by considering the effect of concentration polarization on water flux, may result in higher similarity between simulation and experimental results [19]. For the mesh independency study, the simulation has been performed in two distinct

steps. In the initial step, the accuracy of the mesh near the membrane surface varies from one to 40 layers. For this step, the specifications and obtained results are given in Table 2 and Fig. 3, respectively. The transverse velocity change across the height of membrane channel is considered as a response.

Table 2

Characteristics of the simulations performed to check the mesh independence (variable: number of layers).

| Series | No. of layers | No. of elements | No. of nodes |
|--------|---------------|-----------------|--------------|
| 1 | 1 | 1704 | 562 |
| 2 | 5 | 2016 | 846 |
| 3 | 10 | 3456 | 1551 |
| 4 | 20 | 6336 | 2961 |
| 5 | 30 | 9216 | 4371 |
| 6 | 40 | 12096 | 5781 |

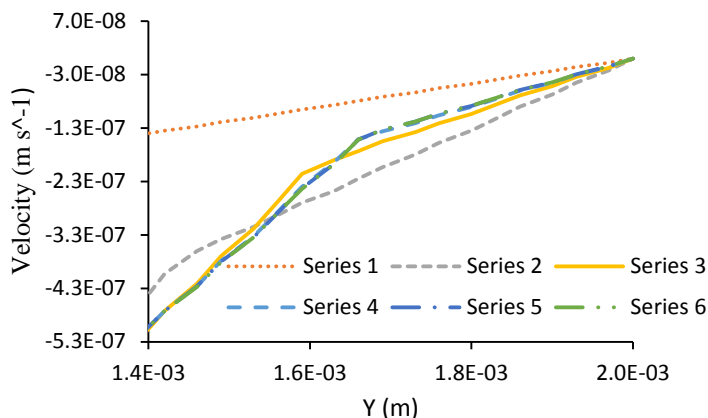


Figure 3. Comparison of the transverse velocity distribution at $x = 0.24$ m across the membrane height (variable: number of layers).

By increasing the number of layers close to the RO membrane surface to more than 20, no changes in the velocity are seen. Therefore, Series 4 is selected for further studies.

At first, the number of optimal layers close to the membrane surface is calculated. In the

following step, the mesh maximum face size was changed, and the number of layers on the membrane surface was kept constant. The characteristics of the new simulations and results are presented in Table 3 and Fig. 4, respectively.

Table 3

Characteristics of the simulations performed to check the mesh independence (variable: maximum mesh size).

| Series | Mesh max. face size (m) | No. of elements | No. of nodes |
|--------|-------------------------|-----------------|--------------|
| 7 | 0.0005 | 24772 | 11760 |
| 8 | 0.001 | 12496 | 5901 |
| 9 | 0.0015 | 8404 | 3948 |
| 4 | 0.002 | 6336 | 2961 |
| 10 | 0.0025 | 5104 | 2373 |
| 11 | 0.003 | 4312 | 1995 |
| 12 | 0.004 | 3256 | 1491 |
| 13 | 0.005 | 2640 | 1197 |
| 14 | 0.007 | 1936 | 861 |

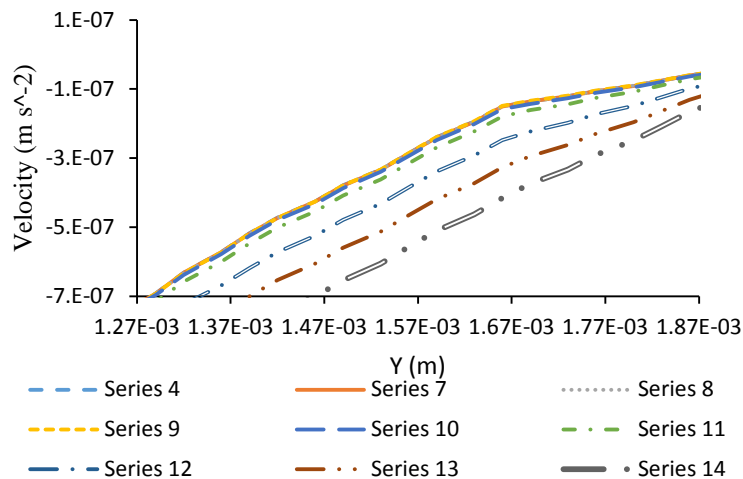


Figure 4. Comparison of the transverse velocity distribution at $x = 0.24$ m across the membrane height (variable: mesh maximum face size).

The results show that with increasing mesh size, the meshing accuracy decreases, which leads to reduced computational load and solving time. As shown in Fig. 4, with a decrease in the maximum mesh size from 0.007 to 0.002 m, the velocity in Y direction converges to the results of simulation Series 4; then, with a decrease of its value to 0.0005, no change is made in the velocity profile.

Thus, the properties of the simulation Series 4 used as a reliable characterization for membrane mesh. In Fig. 5, the membrane chamber is shown by performing a more accurate meshing near the wall.

After designing geometry, meshing, and defining the governing equations and boundary, the simulation of RO modules was done by ANSYS CFX 18.2 software.

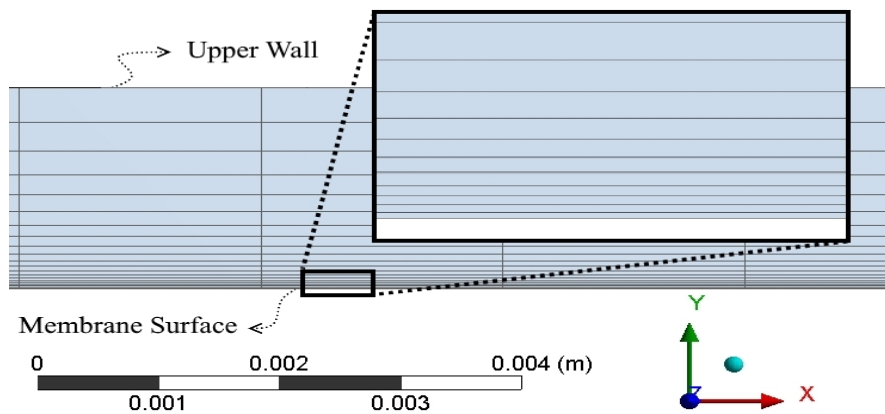


Figure 5. Mesh accuracy near the membrane wall.

2.4. Verification of results

2.4.1. NaCl mass fraction

To investigate the role of physical mechanisms and model verification, the

transverse velocity (Fig. 6) and the mass fraction of salt (Fig. 7) were compared with previous studies that had been validated based on semi-analytical solutions [19-21].

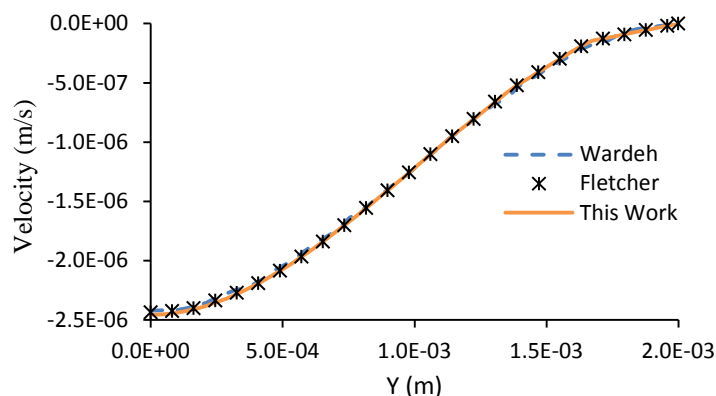


Figure 6. Comparison of the transverse velocity distribution at $x = 0.24$ m against vertical distance from the membrane surface.

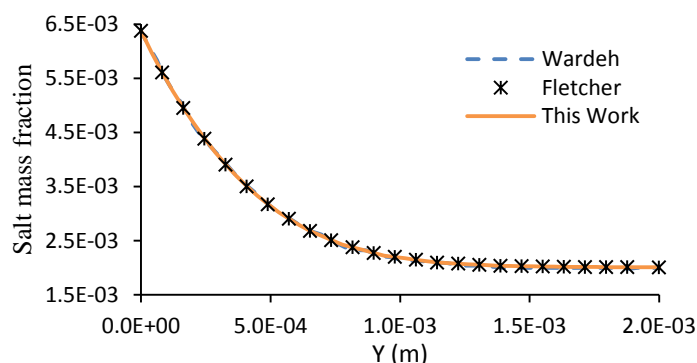


Figure 7. Comparison of the NaCl mass fraction distribution at $x = 0.24$ m against vertical distance from the membrane surface.

The reason for the curved diagrams is that the RO membrane surface is semipermeable,

and the concentration of salt near the membrane should be greater than its mass

fraction near the top surface of the feed channel. The variation manner in transverse velocity and salt concentration at the end of the membrane compartment indicates that the dynamic behavior of the system is correct.

2.4.2. Water permeate velocity and

distribution of NaCl mass fraction on the membrane surface

For a more accurate comparison between this simulation and previous simulations, the water permeate velocity and NaCl mass fraction distribution along the RO membrane are plotted in Fig. 8 and Fig. 9, respectively.

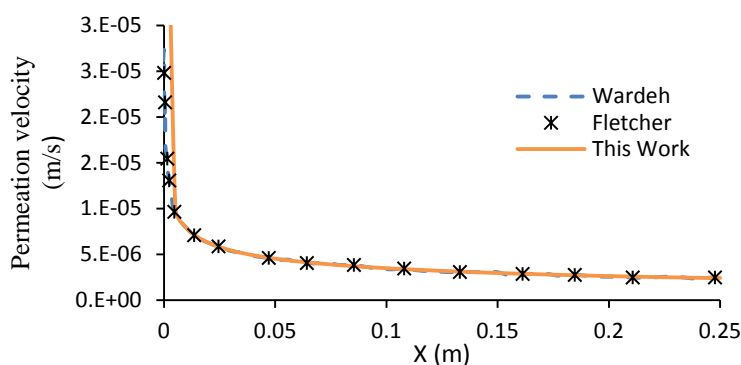


Figure 8. Comparison of water permeate velocity along the membrane.

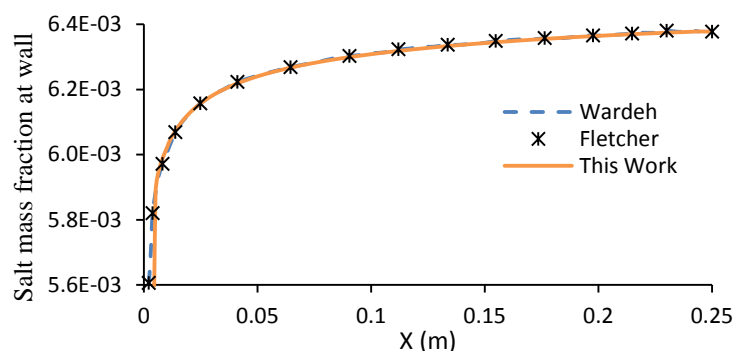


Figure 9. Comparison of NaCl mass fraction distributions along the membrane.

As seen from Figures 9-10, the amount of permeate flux, which is high at the beginning of the channel, gradually decreases due to a reduction in water content and increasing osmotic pressure (which is directly related to the concentration of salt (Eq. 10)). The concentration of salt along the membrane increases due to water permeation into the other side of the membrane.

The model showed good verification with previous studies [19-21]. The major benefit of this model is to consider the concentration polarization and its affecting factors. This feature makes the model more accurate and

reliable to modify in other conditions, like extending it for simulation of different membrane modules.

3. Comparison between different RO membrane modules

To perform an equivalence study, eight different RO membrane channels were compared. In these simulations, the governing conditions, such as flow rate and inlet salt concentration, flow characteristics in the channel, and the absence of gravity force, were considered the same as the primary model, although the coordinates of the

membrane chamber were changed to three-dimensional ones. Where water permeated in Z direction, the conditions for defining the membrane were similar to those defined for Y direction (Section 2.1). For a more accurate comparison of the performances of these eight channels, the membrane area, length, and the inlet mass flow rate were assumed to be the same for all. Some added assumptions are as follows:

- The RO membrane rejection was considered 99 %.
- Due to the changes in the inlet area in membrane chambers, the constant inlet mass flow rate was employed instead of using velocity profile. In the previous simulation, a velocity profile was used at the inlet. For checking the effect of this assumption, two simulations were done by employing a normal mass flow

rate and velocity profile (Fig. 10). It was found that the profile of salt mass fraction was identical, because two different enclosures were considered before (20 mm in length) and after (10 mm in length) the membrane area. These enclosures provided enough time for the development of the flow. Therefore, a normal mass flow rate was defined at the membrane channel inlet.

- The inlet flow rate was considered as 0.00016 kg/s for the five first channels; however, for the others, relative to the decrease of cylinder's diameter, the inlet flow was also reduced (Table 4).
- Dimensions of the primary channel are selected according to the reference [14].

The two membrane chambers and the geometric information of the simulations are depicted in Fig. 11 and Table 4, respectively.

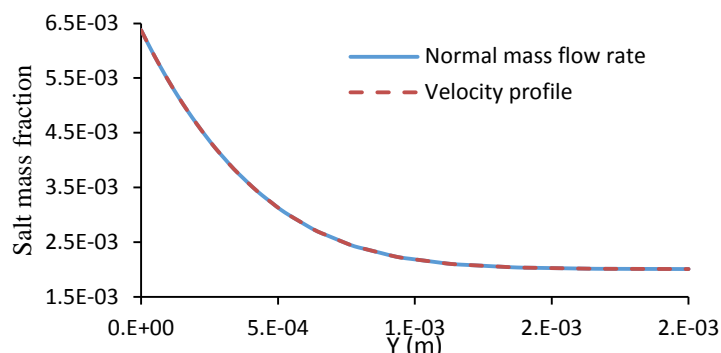


Figure 10. Comparison of the NaCl mass fraction distribution at $x = 0.24$ m against vertical distance from membrane surface (the use of normal mass flow rate and velocity profile).

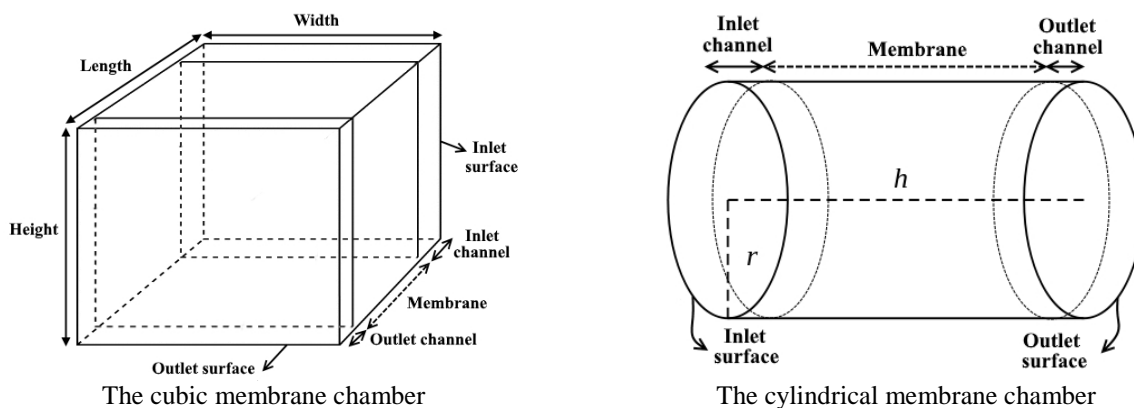


Figure 11. Two membrane chambers.

Table 4

The geometric information of the simulations. For all of these simulations, the length of membrane is 80 mm.

| Series | The membrane placement | Width (mm) | Height (mm) | Radius (mm) | Inlet flow rate (kg/s) | Membrane area (mm ²) |
|------------------------------|--------------------------------------------------------|------------|-------------|-------------|------------------------|----------------------------------|
| Flat sheet membranes | | | | | | |
| 1 | Down surface of the rectangular cube (primary channel) | 40 | 2 | - | 0.00016 | 3200 |
| 2 | Up and down surfaces of the rectangular cube | 20 | 2 | - | 0.00016 | 3200 |
| 3 | Four sides of the rectangular cube | 18 | 2 | - | 0.00016 | 3200 |
| 4 | Four sides of the cube with a square cross-section | 10 | 10 | - | 0.00016 | 3200 |
| Cylindrical membranes | | | | | | |
| 5 | Reference cylinder (R_{ref}) | - | - | 6.37 | 0.00016 | 3200 |
| 6 | Cylinder $R=1/2 \times R_{ref}$ | - | - | 3.18 | 0.00008 | 1600 |
| 7 | Cylinder $R=1/3 \times R_{ref}$ | - | - | 2.12 | 0.000533 | 1066.6 |
| 8 | Cylinder $R=1/4 \times R_{ref}$ | - | - | 1.59 | 0.00004 | 800 |

4. Results and discussion

To compare the simulations, the pressure drop, mass flow rate, Concentration Polarization Layer Thickness (CPLT), and permeation velocity across the RO membrane were investigated.

4.1.1. The permeation mass flow rate

To calculate the flow rate of permeated water and salt, the mass conservation law and the

mass balance equations for water and sodium chloride are used. A portion of water/salt permeates to the other side of the RO membrane, and the greater part of it exits the outlet. As a result, by writing the mass balance equations and considering 99 % rejection for the membrane, the rate of permeated water is calculated and given in Table 5.

Table 5

The flow rate of permeated water and the Mass flow average of inlet velocity in different simulations.

| Series | The flow rate of permeated water (kg/s) | The mass flow average of inlet velocity (m/s) |
|--------|-----------------------------------------|-----------------------------------------------|
| 1 | 1.84E-05 | 0.0018 |
| 2 | 2.31E-05 | 0.0037 |
| 3 | 2.26E-05 | 0.0044 |
| 4 | 1.04E-05 | 0.0016 |
| 5 | 9.47E-06 | 0.0012 |
| 6* | 1.45E-05 | 0.0025 |
| 7* | 1.85E-05 | 0.0038 |
| 8* | 2.17E-05 | 0.005 |

* The amount of flow was reduced.

As mentioned before, in the simulations of 6-8, the amount of flow was reduced because

the diameter and the inlet mass flow were reduced. Thus, for these simulations, the amount of permeated mass flow rate was multiplied by two, three, and four, respectively).

The results show that in the constant inlet mass flow rate and the same membrane surface, the change of geometry is an effective factor in variations in the permeation velocity through the membrane. In Simulations 5-8, the results of increasing the flow velocity due to the decreasing diameter are apparent on the flow rate of permeated water. In addition, a comparison of the first four simulations and four-second simulations implies that only the increase of feed flow rate is not effective in the amount of permeation. Even so, how the water contact with the membrane surface also affects it. Consequently, in Simulations 2 or 3, although the flow rate is less than that of Simulation 8, the amount of permeated water is higher. This is similar to the same phenomenon that

happens by using spacers in the membrane chambers, where creating more turbulence leads to a decrease in the concentration polarization, yet increases the amount of permeate flow rate and pressure drop [9-23].

4.1.2. Pressure drop in the feed channel

The next influential parameter to be compared between simulations is the effect of RO membrane geometry on the pressure drop. This parameter is important because the excessive increase of the pressure drop is directly related to the overall cost for the RO system, especially in the cost of feed and the permeate pumps [24]. Moreover, high pressure drop leads to inadequate system performance [25]. On the other hand, the pressure drop in the feed channel is one of the basic parameters for comparing the accuracy of the results of computer models with large-scale desalination units [26]. The results of different simulations for RO modules are shown in Fig. 12.

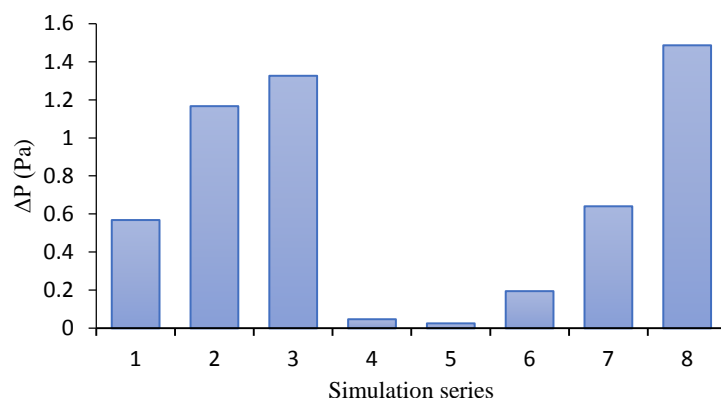


Figure 12. Comparison of the pressure drop in RO membrane chambers for eight simulations.

Since the pressure drop in the chamber is related to the cross-sectional area and the rate of entry into the membrane (Hagen-Poiseuille equation [27]), the changes of these parameters lead to a change in the pressure drop. As shown in Fig. 12, in the simulations of 4 and 5, areas of the chamber's inlet in such

a way produce the least pressure drop.

Based on the results of the pressure drop and the flux of permeated water in eight different simulations, it is possible to make a comparison between distinct geometries of the RO membrane. For example, the pressure drop and the mass flow rate of the permeated

water in a cubic chamber with a rectangular cross-section (the third simulation) can be about equal to the pressure drop of a cylindrical chamber whose diameter is 1/4 diameter of the reference cylinder (the eighth simulation). A similar event occurs for Simulations 1 and 7. On the other hand, by comparing Simulations 6-8, it was found that by decreasing the diameter of the RO membrane chamber, the pressure drop increases. In other words, by decreasing the diameter of the cylinder to the diameter of the hollow fiber membrane (less than 0.5 mm [28]), the pressure drop is increasing, yet the amount of permeated water also increases. Therefore, a trade-off calculation is necessary in order to select the best configuration for the specified conditions.

After all, by considering the flow rate of the permeated water, the pressure drop, the convenience of the instruction membrane module, the flat sheet membrane, Series 2 or the cylindrical membrane geometry with a roughly similar function, Series 8 has a better ability to be used.

4.1.3. CPLT and water permeation velocity

The thickness of the concentration polarization layer, formed near the membrane, can be calculated by the film layer

theory (Eq. 14) [29]:

$$CPLT = \ln\left(\frac{m_{Aw}-m_{Ap}}{m_{A0}-m_{Ap}}\right) \times \frac{D_{AB}}{v_w} \tag{14}$$

The rate of water permeation through the membrane is also obtained by Eq. (5). Due to the water permeation, the thickness of the concentration polarization layer gradually increases along the membrane (Fig. 13). As a result, increasing salt concentration in this area reduces the rate of water permeation along the membrane (Fig. 14). The rate of NaCl mass fraction change along the membrane chamber is compared in Simulations 3 and 8; the result is presented in Fig. 15. As expected, simulation’s results showed that by moving toward the outlet, due to the water permeation, the amount of NaCl mass fraction and CPLT increases near the membrane surface. The higher permeation rate through the membrane results in the lower thickness of the boundary layer due to the salt concentration increase. On the other hand, changes in membrane geometry can result in a higher inlet velocity and pressure drop that leads to a larger permeation velocity, thus reducing the thickness and increasing the compactness of the concentration polarization layer [29].

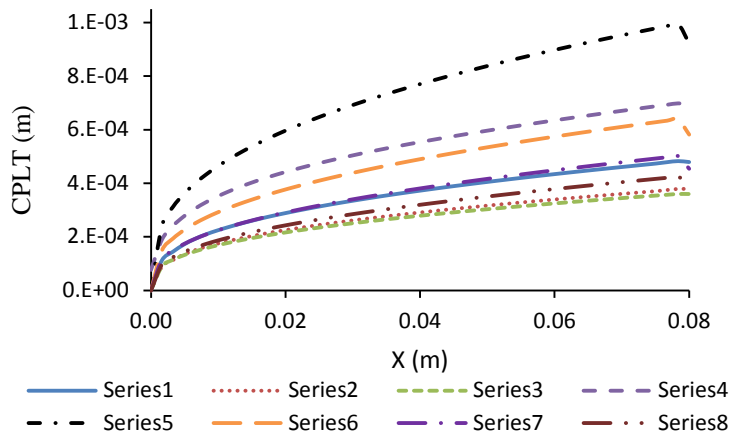


Figure 13. The amount of CPLT along the membrane for eight simulations

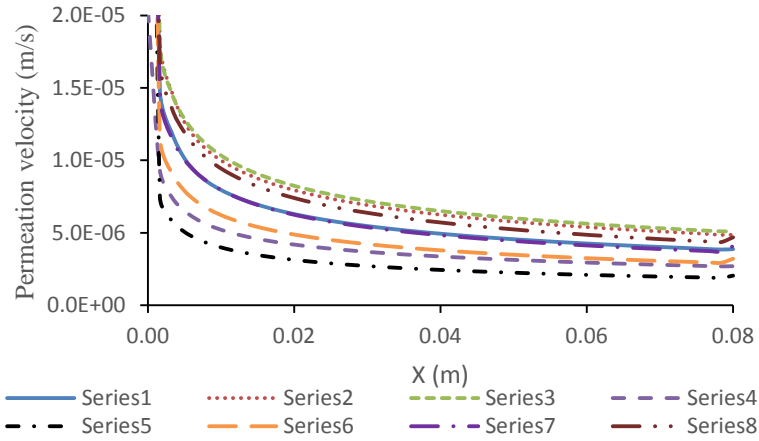
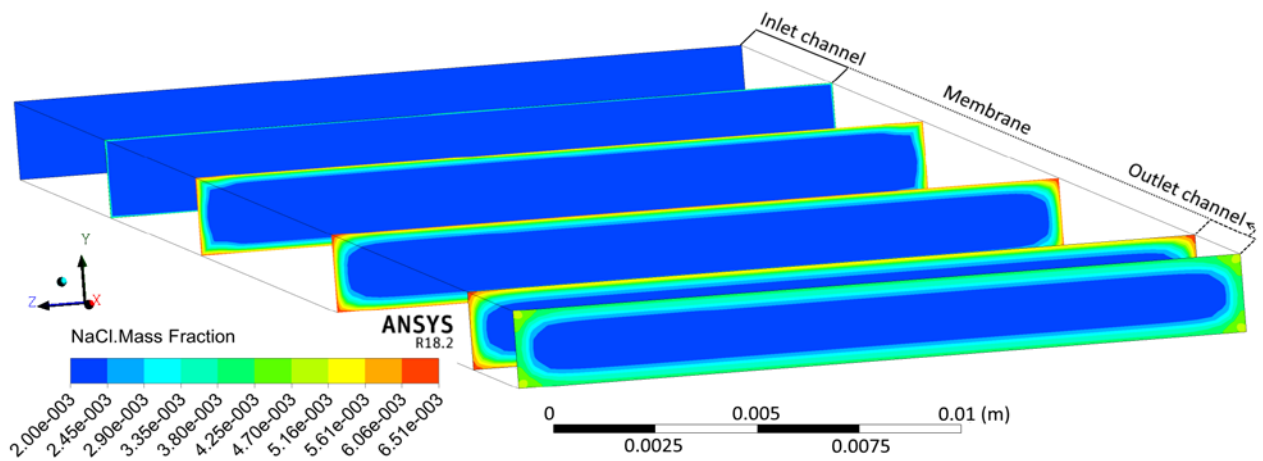
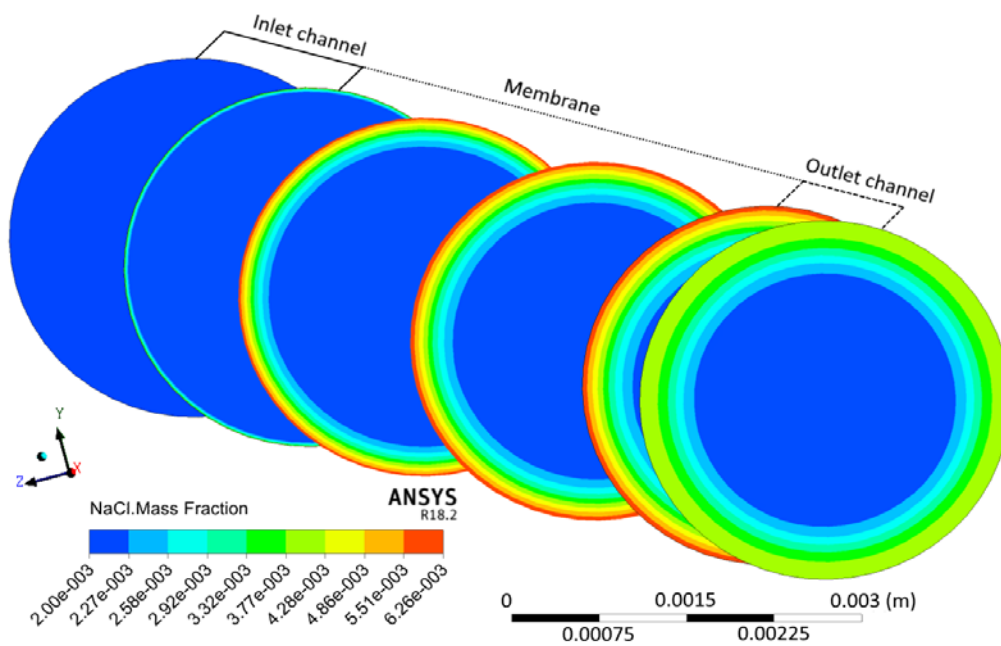


Figure 14. Comparison of the water permeation velocity along the membrane for eight simulations



A. simulation series 3



B. simulation series 8

Figure 15. The contours of NaCl mass fraction along the RO membrane chamber: A. series 3 and B. series 8.

As shown in Figures 13 and 14, the rate of water permeation along the membrane decreases continuously. When the length of the membrane is greater than 0.02 m, these changes tend to be constant in proportion to the geometry and conditions governing the flow. This phenomenon occurs due to the lack of concentration polarization formation at the entrance of the membrane and its increase throughout it. These results also indicate that a large part of the water is permeated in the first parts of the membrane. In addition, excessive membrane length does not have much effect on the permeating water; in contrast, it increases the pressure drop and the cost of pumping and occupies more space by the overall membrane module.

5. Conclusions

In RO simulation, the primary goal is to reduce the difference between experimental data and simulation's results. To achieve this goal, among various numerical techniques that have been used, solution diffusion has been more successful. In this study, contrary to previous researches, comparisons between different membrane compartments in the same operating conditions were performed using the CFD method. The results showed that the tubular membranes could allow more water to pass in the case of diminishing the diameter and increasing the number of tubes. Furthermore, the other advantages of these membranes include an easy procedure to build, reducing ECP due to the movement of tubes, and producing turbulence. The main application of the research becomes quite handy when choosing the type of membrane consumed in the units of water desalination.

It should be noted that despite the above mentioned information, the main assumption of this research and other simulations that

have been done so far, regardless of the effects of temperature, ultimately leads to a reduction in the range of applications of simulation results. Due to the effects of temperature, especially on the flow rate of water from the membrane, in future studies, it is better to see these effects in calculating the operational parameters affecting water permeation (density, molecular diffusion coefficient, osmotic pressure, and viscosity).

Nomenclature

| | |
|-----------|----------------------------------------------------------------------------------------------------|
| D_{AB} | the diffusion coefficient of salt in water [m ² s ⁻¹]. |
| g | the gravity [m s ⁻²]. |
| h | height of feed channel [m]. |
| k | constant based only on the permeation flux of pure solvent [m s ⁻¹ Pa ⁻¹]. |
| l | length of membrane [m]. |
| m_A | the mass fraction of the salt [kg solute per kg of solution]. |
| m_{Ap} | the mass fraction of the salt on the permeate side of the membrane [kg solute per kg of solution]. |
| m_{Aw} | the mass fraction of the salt on the feed side of the membrane [kg solute per kg of solution]. |
| m_{A0} | the mass fraction of the salt applied at the inlet [kg solute per kg of solution]. |
| P | pressure [Pa]. |
| R | rejection coefficient. |
| u | the velocity component in X direction [along the channel] [m s ⁻¹]. |
| \bar{u} | the mean flow velocity at the entrance of the feed channel [m s ⁻¹]. |
| v | the mean velocity component in Y direction (normal to the membrane) [m s ⁻¹]. |

Greek letters

| | |
|-------------|----------------------------------------------------|
| $\Delta\pi$ | osmotic pressure differential across the membrane. |
| π | osmotic pressure of the aqueous solution [Pa]. |
| μ | viscosity [Pa s]. |
| ρ | fluid density [kg m ⁻³]. |

References

- [1] Liu, Q., Liu, C., Zhao, L., Ma, W., Liu, H. and Ma, J., "Integrated forward osmosis-membrane distillation process for human urine treatment", *Water Research*, **91**, 45 (2016).
- [2] Lin, S., "Mass transfer in forward osmosis with hollow fiber membranes", *Journal of Membrane Science*, **514**, 176 (2016).
- [3] Coday, B. D., Xu, P., Beaudry, E. G., Herron, J., Lampi, K., Hancock, N. T. et al., "The sweet spot of forward osmosis: Treatment of produced water, drilling wastewater, and other complex and difficult liquid streams", *Desalination*, **333** (1), 23 (2014).
- [4] Porter, M. C., Handbook of industrial membrane technology, Noyes Publications, Park Ridge, NJ, USA, (1989).
- [5] El-Dessouky, H. T. and Ettouney, H. M., Fundamentals of salt water desalination. Elsevier Science, (2002).
- [6] Gu, B., Adijman, C. S. and Xu, X. Y., "The effect of feed spacer geometry on membrane performance and concentration polarisation based on 3D CFD simulations", *Journal of Membrane Science*, **527**, 78 (2017).
- [7] Koutsou, C. P. and Karabelas, A. J., "Shear stresses and mass transfer at the base of a stirred filtration cell and corresponding conditions in narrow channels with spacers", *Journal of Membrane Science*, **399–400**, 60 (2012).
- [8] Koutsou, C. P., Yiantsios, S. G. and Karabelas, A. J., "A numerical and experimental study of mass transfer in spacer-filled channels: Effects of spacer geometrical characteristics and Schmidt number", *Journal of Membrane Science*, **326** (1), 234 (2009).
- [9] Fimbres-Weihs, G. A. A. and Wiley, D. E. E., "Review of 3D CFD modeling of flow and mass transfer in narrow spacer-filled channels in membrane modules", *Chemical Engineering and Processing: Process Intensification*, **49** (7), 759 (2010).
- [10] Darcovich, K., Dalcin, M. and Gros, B., "Membrane mass transport modeling with the periodic boundary condition", *Computers & Chemical Engineering*, **33** (1), 213 (2009).
- [11] Verliefde, A. R. D., Van der Meeren, P. and Van der Bruggen, B., Solution-diffusion processes, Encyclopedia of membrane science and technology, (1), pp. 1 (2013).
- [12] Wijmans, J. G. H. and Baker, R. W., The solution-diffusion model: A unified approach to membrane permeation, In: Materials science of membranes for gas and vapor separation, John Wiley & Sons Ltd., Chichester, UK, pp. 159 (2006).
- [13] Wijmans, J. G. and Baker, R. W., "The solution-diffusion model: A review", *Journal of Membrane Science*, **107** (1–2), 1 (1995).
- [14] Gruber, M. F., Aslak, U. and Hélix-Nielsen, C., "Open-source CFD model for optimization of forward osmosis and reverse osmosis membrane modules", *Separation and Purification Technology*, **158**, 183 (2016).
- [15] Gruber, M. F., Johnson, C. J., Tang, C., Jensen, M. H., Yde, L. and Helix-Nielsen, C., "Validation and analysis of forward osmosis CFD model in complex 3D geometries", *Membranes*, **2** (4), 764 (2012).
- [16] Harasek, M., Haddadi, B., Miltner, M., Schretter, P. and Jordan, C., "Fully

- resolved CFD simulation of a hollow fibre membrane module”, *Chemical Engineering Transactions*, **52**, 433 (2016).
- [17] Jones, L. and Achilli, A., Three-dimensional CFD models of hybrid reverse osmosis systems, Humboldt State University, (2015).
- [18] Baker, R. W., Membrane technology and applications, John Wiley & Sons Ltd., Chichester, UK, (2004).
- [19] Wardeh, S. and Morvan, H. P. P., “CFD simulations of flow and concentration polarization in spacer-filled channels for application to water desalination”, *Chemical Engineering Research and Design*, **86** (10), 1107 (2008).
- [20] Geraldes, V. V., Semião, V. and De Pinho, M. N., “Flow and mass transfer modelling of nanofiltration”, *Journal of Membrane Science*, **191** (1–2), 109 (2001).
- [21] Fletcher, D. F. and Wiley, D. E., “A computational fluids dynamics study of buoyancy effects in reverse osmosis”, *Journal of Membrane Science*, **245** (1–2), 175 (2004).
- [22] Jamal, K., Khan, M. A. and Kamil, M., “Mathematical modeling of reverse osmosis systems”, *Desalination*, **160** (1), 29 (2004).
- [23] Subramani, A., Kim, S. and Hoek, E. M. V., “Pressure, flow, and concentration profiles in open and spacer-filled membrane channels”, *Journal of Membrane Science*, **277** (1–2), 7 (2006).
- [24] Ahmad, A. L. and Lau, K. K., “Impact of different spacer filaments geometries on 2D unsteady hydrodynamics and concentration polarization in spiral wound membrane channel”, *Journal of Membrane Science*, **286** (1–2), 77 (2006).
- [25] Schwinge, J., Neal, P. R., Wiley, D. E., Fletcher, D. F. and Fane, A. G., “Spiral wound modules and spacers”, *Journal of Membrane Science*, **242** (1–2), 129 (2004).
- [26] Mancha, E., DeMichele, D., Walker, W. S., Seacord, T. F., Sutherland, J. and Cano, A., Part II: Performance evaluation of reverse osmosis membrane computer models by Texas Water Development Board, Austin, Texas, 78711-3231, (2014).
- [27] Sutera, S. P. and Skalak, R., “The history of Poiseuille’s law”, *Annual Review of Fluid Mechanics*, **25** (1), 1 (1993).
- [28] Drioli, E. and Giorno, L., Encyclopedia of membranes, Heidelberg: Springer Berlin, Berlin, (2016).
- [29] Ahmad, A. L., Lau, K. K., Bakar, M. Z. A. and Shukor, S. R. A., “Integrated CFD simulation of concentration polarization in narrow membrane channel”, *Computers & Chemical Engineering*, **29** (10), 2087 (2005).